Trends in Biotechnology

CellPress
OPEN ACCESS

Research Article

Efficiency and process development for microbial biomass production using oxic bioelectrosynthesis

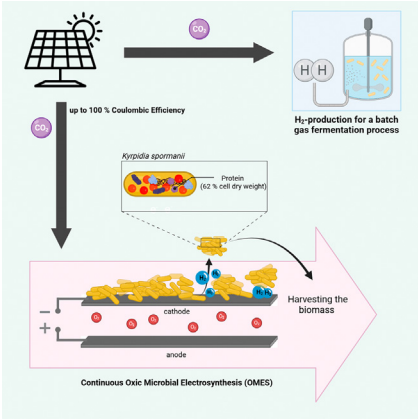

Oxic microbial electrosynthesis (OMES) using *Kyrpidia spormannii* can match the electron efficiency of gas fermentation, without producing explosive gas mixtures. It uses solar energy efficiently and has the potential to produce complex products, such as proteins, for food and feed instead of methane and alcohols, which are typical products of anoxic MES.

Leonie Rominger, Max Hackbarth, Tobias Jung, Marvin Scherzinger, Luis F.M. Rosa, Harald Horn, Martin Kaltschmitt, Cristian Picioreanu, Johannes Gescher

Johannes.gescher@tuhh.de
(J. Gescher).

Highlights

By using carbon dioxide (CO_2) as carbon source, fossil sources can be replaced. In microbial electrosynthesis (MES), CO_2 and *in situ* produced hydrogen (H_2) are used for bacterial biofilm growth.

Kyrpidia spormannii is a Knallgas bacterium with a protein content of 61% of its dry mass. It grows as a biofilm on the cathode in an oxic MES. The biomass can be used for the food and feed industry.

A continuous process was established by applying a negative potential to harvest parts of the biofilm for use. The biofilm regenerated after being partly harvested.

The system was operated at maximum coulombic efficiency, enabling the energy input to be minimized.

A numerical model describing the growth of *K. spormannii* as a H_2-oxidizing bacterium in an oxic MES system was developed. This helps predict growth behavior and efficiencies for further optimization.

Trends in Biotechnology, March 2025,
Vol. 43, No. 3
https://doi.org/10.1016/j.tibtech.2024.11.005

CellPress
OPEN ACCESS

Trends in
Biotechnology

Research Article

Efficiency and process development for microbial biomass production using oxic bioelectrosynthesis

Leonie Rominger[1], Max Hackbarth[2], Tobias Jung[3], Marvin Scherzinger[4], Luis F.M. Rosa[5], Harald Horn[2], Martin Kaltschmitt[4], Cristian Picioreanu[5], and Johannes Gescher[1,*]

Autotrophic microbial electrosynthesis (MES) processes are mainly based on organisms that rely on carbon dioxide (CO_2) as an electron acceptor and typically have low biomass yields. However, there are few data on the process and efficiencies of oxic MES (OMES). In this study, we used the knallgas bacterium *Kyrpidia spormannii* to investigate biomass formation and energy efficiency of cathode-dependent growth. The study revealed that the process can be carried out with the same electron efficiency as conventional gas fermentation, but overcomes disadvantages, such as the use of explosive gas mixtures. When accounting only for the electron input via electrical energy, a solar energy demand of 67.89 kWh kg^{-1} dry biomass was determined. While anaerobic MES is ideally suited to produce methane, short-chain alcohols, and carboxylic acids, its aerobic counterpart could extend this important range of applications to not only protein for use in the food and feed sector, but also further complex products.

Introduction

Increased atmospheric CO_2 concentrations and consequent climate changes are significant challenges for human development [1–4]. Addressing this problem necessitates transformation of the global economy. The substrate bases used for technical processes need to be shifted toward biobased organic substrates or CO_2. Technical solutions exist for reducing CO_2 with electrolysis-derived hydrogen (H_2), and then converting this carbon into long-chain hydrocarbon molecules [5–7]. In addition to such heat-induced chemical processes, biological catalysis using basically the same feedstock is also able to produce long-chain hydrocarbons. Compared with thermochemical processes, these biological processes typically operate under milder conditions, require less energy, and can direct organisms toward producing a range of precisely defined end products [8–11].

Reducing CO_2 in natural fixation cycles requires energy and reducing equivalents [12]. In biotechnology, H_2 is the most common energy source and electron donor for CO_2-based processes that do not use photosynthetic organisms [13]. Nevertheless, both process strategies have certain challenges. H_2 exhibits low solubility in water, which hinders its application in achieving competitive space–time yields, or necessitates significant energy input for the mixing and homogeneous distribution of small H_2 bubbles. Nevertheless, under certain circumstances, commercial application of anaerobic gas fermentation is feasible, especially using side streams, such as from the steel industry, for example. Contemporary water electrolysis can be utilized for H_2 production. However, the energy efficiency of this process currently stands at 70%, and it typically relies on expensive membranes to separate the anode and cathode compartments and, at least in

Technology readiness

Oxic microbial electrosynthesis (OMES) is a relatively new technology, particularly in the context of biofilm-based processes, which is now achieving a Technology Readiness Level (TRL) of 3 in laboratory reactors. Similar to other biofilm-based technologies, OMES faces both challenges and opportunities. One of the primary challenges will be identifying a reactor design that maximizes electrode surface area while simultaneously maintaining a predictable fluidic regime. Since OMES relies on an electrochemical system, reactor configuration must also minimize electrochemical losses. If biomass is intended to be the end product, it is important to consider that, over the duration of the experiment, microorganisms are likely to adapt to the changing process conditions, potentially enabling evolution-based optimization of biocatalysts. In the future, OMES is likely to compete with processes relying on anaerobic gas fermentation as a first step and subsequent usage of end products from this first step as feed for a second reaction step likely involving aerobic microorganisms. Full economic and ecological process assessment based on larger scale reactors will be necessary to decide under which circumstances which technology might be superior.

[1]Institute of Technical Microbiology, Hamburg University of Technology (TUHH), Kasernenstraße 12 (F), 21073 Hamburg, Germany
[2]Engler-Bunte-Institut, Water Chemistry and Water Technology, Karlsruhe Institute of Technology (KIT), Engler-Bunte-Ring 9, 76131 Karlsruhe, Germany

 https://doi.org/10.1016/j.tibtech.2024.11.005

some installations, noble electrodes [14,15]. However, membrane biofilm reactors using hollow fiber membranes provide a scalable reactor system for biofilm-based gas fermentation that can avoid the gas solubility problem if sufficient energy for water electrolysis is available [16]. By contrast, photosynthesis requires substantial space for adequate illumination. Moreover, if sunlight is intended to be used directly and light is not provided using, for instance, light-emitting diodes (LEDs), the productivity of such systems will vary significantly based on latitude.

A relatively recent development in the field of energy conversion for biological CO_2 capture and utilization is **MES** (see Glossary) [17]. In MES, microorganisms interact with a solid-state cathode serving as an energy and electron source. Energy and electron transfer can occur directly or with H_2 produced on the cathode surface [13,18]. The latter appears to be the case for the bacterium *K. spormannii*, which was used in the current study (T. Jung, PhD thesis, Karlsruher Institut für Technologie, 2020) [19]. Nevertheless, there is also evidence that enzymes involved in sulfur oxidation might also have a role in electron transfer reactions from the cathode surface to the cytoplasmic membrane of the organism [20]. The most effective interaction mode in MES is the formation of a microbial **biofilm** directly on the electrode surface [21]. MES can be highly efficient, due to the biological functionalization of the cathode surface, the constant depletion of H_2, the enzymatic catalysis of H_2 production through direct enzyme–electrode interactions, and/or the direct enzyme-mediated electron import into the respiratory chain of the organism [22,23]. Consequently, there is no need for expensive electrode materials, at least on the cathode side, due to biological material functionalization. If the organisms utilize H_2 produced on the cathode surface, the process can be directed toward complete depletion during diffusion through the biofilm, effectively circumventing the issue of H_2 solubility in water through process control. Along these lines, recent results suggest that volumetric production rates comparable with industrial syngas and chain elongation fermentation reactions can be achieved via MES [24].

Currently, most MES processes are carried out by anaerobic organisms, specifically acetogens and methanogens. These anoxic processes exhibit high electron efficiencies, and their production of a variety of value-added substances has been shown. For instance, cathode-dependent methane production (also called electromethanogenesis [25]) was found to have very high **Coulombic efficiencies (CEs)** in a variety of studies [26,27]. Moreover, life-cycle assessment revealed that upcycling of biogas, which is typically a mixture of 50% H_2 and 50% methane, toward 100% methane content can be more efficient if the biogas process is coupled to electromethanogenesis instead of a power-to-gas process [28]. MES with acetogens can yield a product spectrum comparable with that achievable with H_2/CO_2-based gas fermentation, comprising short-chain fatty acids and their corresponding alcohols [29–32]. Chain length can be increased using separate chain elongation steps. Recent results also point toward the production of further products, such as ethanolamine or glycine using Clostridia as biocatalysts [33]. In addition, because several species of Clostridia can fix nitrogen, MES with these organisms, among others, was presented as one possibility for nitrogen fixation to ammonia, which could help reduce the amount of energy needed for Haber–Bosch-based ammonia production. Nevertheless, methanogens and acetogens also have disadvantages as biocatalysts for bioelectrosynthesis processes. Genetic engineering of these organisms is challenging, and the end-product spectrum is limited due to energy constraints. This includes biomass and protein as potential end products, because biomass yield coefficients are also consequently low [34–36]. In addition, a membrane is required to separate the anode and cathode in the reactor systems, posing challenges in terms of their construction.

Recently, aerobic bacteria have been introduced into MES processes, potentially offering several advantages [37–39]. These organisms thrive using a process that is highly exergonic. The

[3]Department of Applied Biology, Institute for Applied Biosciences, Karlsruhe Institute of Technology (KIT), Fritz-Haber-Weg 2, 76131 Karlsruhe, Germany
[4]Institute of Environmental Technology and Energy Economics, Hamburg University of Technology (TUHH), Eissendorfer Str. 40 (N), 21073 Hamburg, Germany
[5]Water Desalination and Reuse Center (WDRC), Biological and Environmental Science and Engineering Division (BESE), King Abdullah University of Science and Technology (KAUST), Thuwal, 23955-6900, Kingdom of Saudi Arabia

*Correspondence:
Johannes.gescher@tuhh.de
(J. Gescher).

increased energy availability provides greater flexibility for genetic engineering of their metabolism, enabling the production of a diverse array of end products. Additionally, biomass growth rates are higher compared with acetogens and methanogens, and the production of single cell protein as a viable product appears feasible [40,41].

A lack of fundamental information regarding the energy efficiency of OMES processes hinders their future development. This is especially true for biofilm-based processes, although some authors have already reported polyhydroxybutyrate production using OMES in a process operating with planktonic cells [38]. In addition, if biomass is intended to be a product of an OMES biorefinery, it remains unclear how the biomass cultivated on the cathode can be harvested continuously.

To address these questions, this study utilized the recently isolated thermoacidophilic **knallgas** bacterium *K. spormannii* [19,42]. Biomass growth rates on cathode surfaces were assessed using **optical coherence tomography (OCT).** CE was determined and correlated with electrode coverage. A process model was established allowing the description of the process and the adjustment of oxygen (O_2) levels according to the demands of the organism. The energy efficiency of OMES was compared with the efficiencies of the following: biotechnological conversion of H_2 produced by water electrolysis, as well as oxygenic photosynthesis for microalgae, **C_3** and **C_4 plants**. The results indicated competitive energy efficiency compared with plant photosynthesis and the two-step process, providing a basis for evidence-based decision-making in the development of OMES for future applications in energy conversion, and CO_2 utilization and capture. Furthermore, this study demonstrates the feasibility of continuous biofilm-based processes on cathodes through the intermittent shearing of biomass from the electrode by forming H_2 bubbles.

Results

Growth kinetics of *K. spormannii* biofilms on cathode surfaces at different applied potentials

First, the effect of the applied potential on biofilm growth and formation was investigated. OCT was used to quantify biovolume. The aim was to analyze the potential window in which growth of *K. spormannii* could be observed. Figure 1A shows the relative biovolume, where the biovolume at each time point was normalized to the maximum biovolume of the respective cultivation. Table 1 summarizes quantitative data of the experiments presented in Figure 1. The trend lines over the data points of each growth curve were modeled using a fourth-order polynomial (R^2 >99%). At 0 mV versus standard hydrogen electrode (SHE), coverage of the electrode was observed, but biomass growth was slow. The average current during the 16 days at 0 mV was –0.65 μA cm^{-2}. By comparison, the average current density at –375 mV and –500 mV was –6.95 μA cm^{-2} and –45.02 μA cm^{-2}, respectively. However, the cells remained viable even after more than 2 weeks at this potential since a switch to –500 mV led to the rapid growth of the organisms on the cathode. Exponential growth started immediately after inoculation at –375 mV (green) and –500 mV versus SHE (blue). The maximum biovolume was reached after ~8 days. Moreover, in terms of accumulation rate (Figure 1B), which represents the derivative of biovolume over time, only minor differences were observed. The maximum accumulation rate at –500 mV versus SHE was observed after 1.8 days, with a value of 62.05 mm^3 day^{-1}, slightly higher than the value of 52.12 mm^3 day^{-1} observed at –375 mV versus SHE after 3.4 days. For all potentials, the maximum accumulation rate was correlated with complete substratum coverage (Figure 1C).

The biofilm morphology varied among the biofilms grown at different potentials. Figure 2 illustrates the biofilm height maps for mature biofilms. To further characterize the biofilm structure, porosity and roughness were calculated using the same potentials as in the previous studies (Table 2). At

Glossary

Biofilm: community of microorganisms that have produced an extracellular polymeric matrix holding the cells together and giving the community a certain set of new characteristics. A biofilm can comprise flocks of cells or cells binding to a solid surface, which is, in this case, called a substratum.
C_3 plants: perform photosynthesis under normal temperature and light conditions. However, in hot and dry weather, they show a decrease in photosynthetic efficiency. In C_3 plants, CO_2 is fixed in the Calvin cycle during the RuBisCO reaction with ribulose-1,5-bisphosphate. An unstable intermediate is formed, which then breaks down into two stable molecules of 3-phosphoglycerate (3-PGA). Since 3-PGA comprises three carbon atoms, these plants are referred to as C_3 plants.
C_4 plants: plants (e.g., maize and sugarcane) that bind CO_2 more efficiently compared with C_3 plants. They have adapted to warmer regions with higher light intensity, such as tropical and subtropical climates. Typically, plants close their stomata at high ambient temperatures to limit water loss through transpiration. However, this action makes it more difficult to uptake CO_2 for photosynthesis. Therefore, C_4 plants have evolved a mechanism to utilize even minimal amounts of CO_2 effectively. In contrast to C_3 plants, the first intermediate product of photosynthesis in C_4 plants, oxaloacetate, comprises four carbon atoms.
Coulombic efficiency (CE): describes the selectivity of a (bio) electrochemical process by quantifying the collected product and comparing it to the potential amount that could be generated from the total charge transferred. It is typically expressed as a percentage.
Knallgas: German term that refers to a mixture of H_2 and O_2 gases.
Microbial electrosynthesis (MES): electricity-driven process in which microorganisms take up electrons either directly or indirectly (e.g., through the production of H_2 as an intermediate) from a cathode surface. Therefore, the cathode serves as an electron and energy source for the microorganisms.
Optical coherence tomography (OCT): uses low-coherence interferometry, wherein a light source emits a beam that is split into two paths:

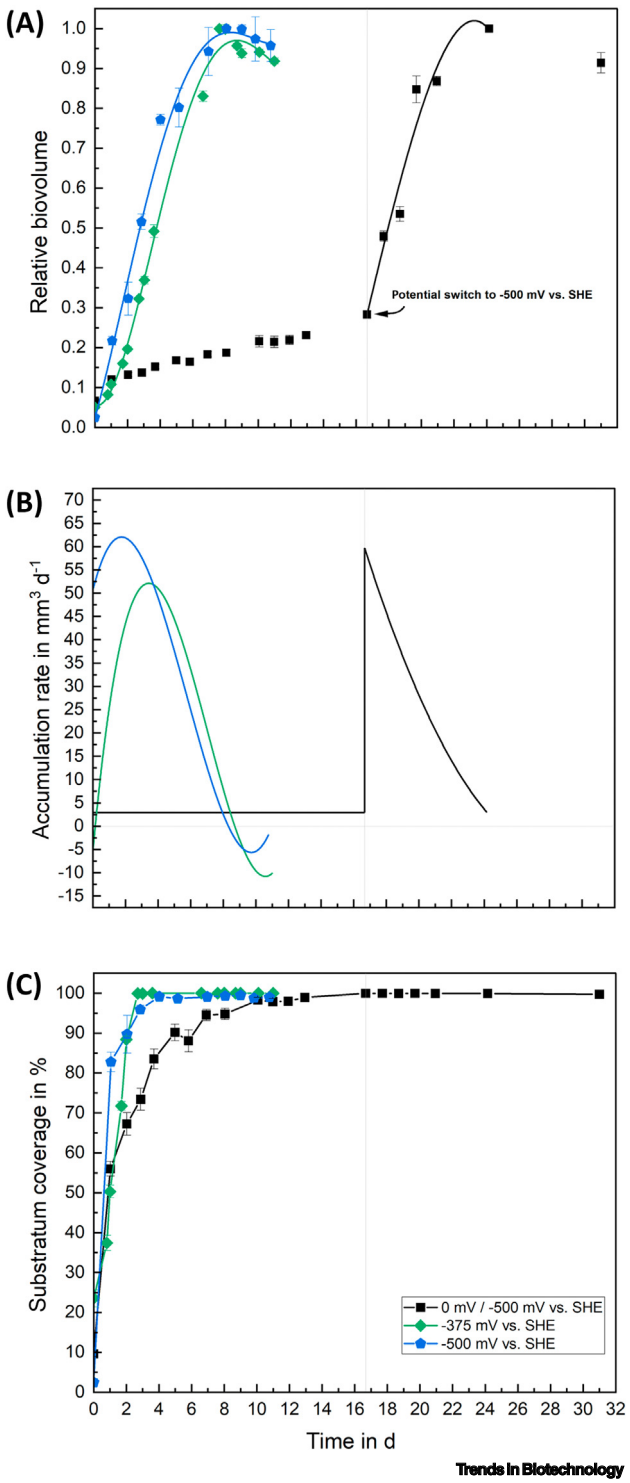

Figure 1. Effects of applied potential on (A) relative biovolume, (B) accumulation rate, and (C) substratum coverage; comparison between growth at –500 mV versus standard hydrogen electrode (SHE) (blue), –375 mV versus SHE (green) and 0 mV versus SHE (switched to –500 mV versus SHE after 16.7 days, respectively) (black). The data show the results from triplicate optical coherence tomography (OCT) data from representative experiments. The error bars represent standard deviations. The experiment at –500 mV was conducted in independent biological triplicate, while the other experiments were conducted in independent duplicates. The accumulation rate was calculated based on growth of the entire biofilm on a surface area of 20 cm^2. Substratum coverage describes the percentage area of the cathode that was covered with biofilm.

one that reflects off the material of interest and another that serves as a reference. When the two beams recombine, they create an interference pattern. By analyzing these patterns, OCT can produce images of the materials at varying depths.

Table 1. Effects of applied potential on normalized biovolume, normalized accumulation rate, and substratum coverage[a]

Feature	Maximum	SD	Time (days)
0 mV/–500 mV versus SHE[b]			
Normalized biovolume ($\mu m^3\ \mu m^{-2}$)	137.1[b]	5.4[b]	24.2[b]
Normalized accumulation rate ($\mu m^3\ \mu m^{-2}\ d^{-1}$)	29.8[b]	Not done	16.7[b]
Substratum coverage (%)	99.98[b]	0.01[b]	16.7[b]
–375 mV versus SHE			
Normalized biovolume ($\mu m^3\ \mu m^{-2}$)	152.2	5.0	7.6
Normalized accumulation rate ($\mu m^3\ \mu m^{-2}\ d^{-1}$)	26.1	Not done	3.3
Substratum coverage (%)	99.93	0.05	2.7
–500 mV versus SHE			
Normalized biovolume ($\mu m^3\ \mu m^{-2}$)	172.1	3.2	8.1
Normalized accumulation rate ($\mu m^3\ \mu m^{-2}\ d^{-1}$)	31.0	Not done	1.8
Substratum coverage (%)	99.14	0.16	4.0

[a]The absolute maximum biovolume was 125–175 $\mu m^3\ \mu m^{-2}$ for all cultivations.
[b]Values that appeared after the switch to –500 mV versus SHE.

–500 mV versus SHE, the biofilms exhibited tower-like structures with dimensions of up to 0.3 mm from the substratum surface. The biofilm had a relatively high porosity, with individual tower-like structures separated by an average distance of 0.5–1 mm from each other. Similar biofilm structures were observed when the potential was shifted from 0 mV versus SHE, where only minor biofilm growth was observed, to –500 mV versus SHE. This finding supports the notion that this growth pattern is robust at this potential. At –375 mV, representing lower energy availability, the biofilms exhibited denser growth and lower porosity. At 0 mV, very short tower-like structures with a mean thickness of 30 µm were observed after 16 days. This was only 20% and 14% of the maximum mean height reached at –375 mV and –500 mV, respectively, after 8 days. An abiotic control did not show similar structures (Figure S3 in the supplemental information online).

Model results

A 1D model was proposed to describe the experimental results and adjust process conditions, aiming to assess process efficiency. The model was able to qualitatively describe the biofilm

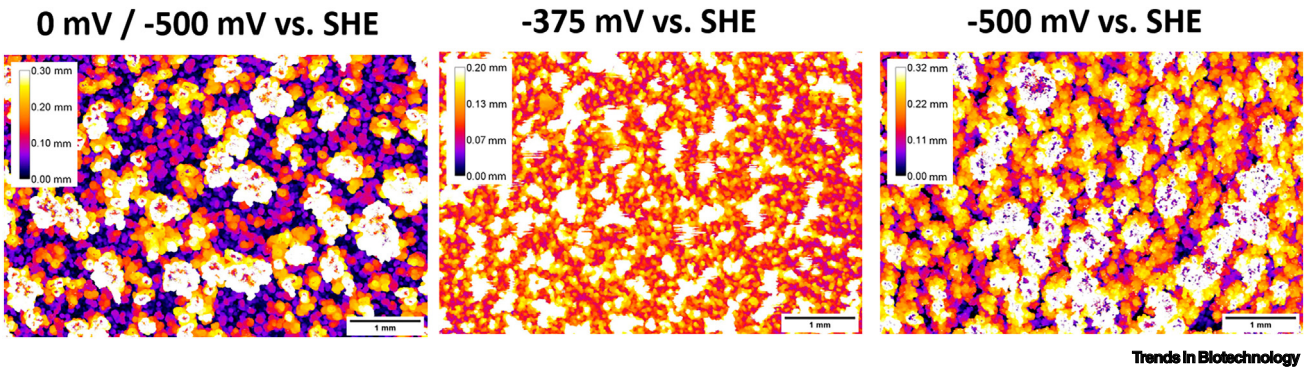

Figure 2. Height maps of biofilms grown at different potentials. The height maps display a top view of the biofilm. The shape of the biofilm correlates with the applied potential. The colors represent the height of the biofilm, the numbers in the color calibration bar are given in mm. The images were taken on Day 31 [0 mV; Day 14.33 (–500 mV)], Day 11 (–375 mV), and Day 10.77 (–500 mV), respectively. Abbreviation: SHE, standard hydrogen electrode.

Table 2. Biofilm porosity and roughness for biofilms grown at different potentials as structure-describing parameters

	0 mV/–500 mV versus SHE[a]	–375 mV versus SHE	–500 mV versus SHE
Porosity (%)	28.87	6.77	24.50
Roughness coefficient (mm)	0.733	0.520	0.518

[a]The calculations were made for Day 31 (0 mV; Day 14.33 at –500 mV), Day 11 (–375 mV), and Day 10.77 (–500 mV), with a switch in potential on Day 16.

growth of *K. spormannii* in the recirculating batch flow cell using the parameters listed in Table S1 in the supplemental information online. The biofilm thickness computed by the model at –500 mV versus SHE is shown in Figure 3 and compared with the experimental data obtained for the same conditions (see Figure 4 for the OMES process). In the model, the gas phase replenishments at several moments in time were introduced to mimic the experimental gas phase exchanges. Liquid and gas phase compositions of H_2, O_2, and CO_2 were computed in time, with changes due to microbial conversion. The model indicated that H_2 was produced sufficiently fast enough to provide energy to the whole growing biofilm, evident from the fact that unreacted H_2 getting through the biofilm accumulated in both liquid (Figure 3A) and gas (Figure 3B) phases until the next gas

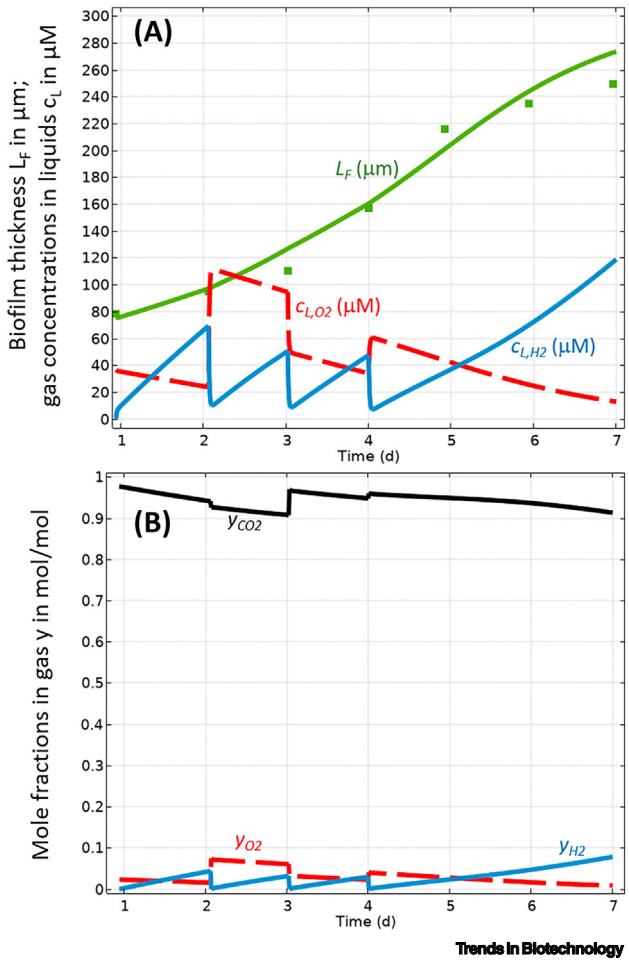

Figure 3. COMSOL-model results. (A) Simulated development of biofilm thickness [green line, model; squares, experimental at –500 mV vs. standard hydrogen electrode (SHE)] and dissolved gas concentrations (O_2, red-broken line, H_2, blue unbroken line). (B) Computed development of gas composition, in mole fractions. The steps correspond to periodical gas-flushing events. CO_2 is supplied in large excess and, thus, is not limiting for biomass growth.

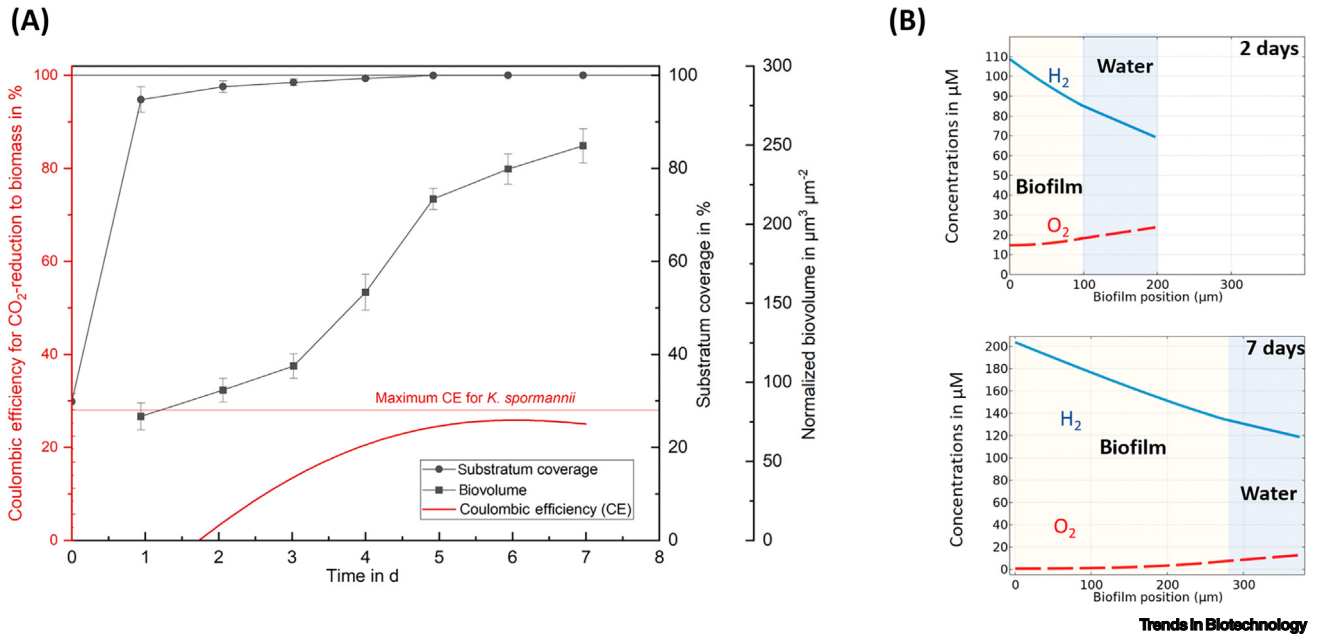

Figure 4. Investigation of growth-limiting and efficiency-determining parameters. (A) Accumulated Coulombic efficiency (CE; red), normalized biovolume (black squares), and substratum coverage (black circles) over time for biofilm growth at –500 mV versus standard hydrogen electrode (SHE); CE for the reduction of CO_2 indicates how many electrons were used for CO_2 reduction to biomass (anabolism only). The data were taken before flushing the headspace with fresh gas. (B) Computed concentration profiles in the biofilm and mass transfer boundary layer, after 2 and 7 days growing at –500 mV versus SHE, showing typical counter-diffusional effects. The yellow-shaded area indicates the biofilm region, while the blue area is the mass transfer boundary layer. CO_2 concentration (not shown here) was not rate limiting and it had an almost constant value corresponding to the bulk liquid concentration. At Day 2, no rate limitation occurred in the ~100 µm-thick biofilm. At Day 7, O_2 near the cathode surface was almost depleted.

exchange event. From Day 1 to Day 4, the biofilm got thicker with no kinetic limitations by H_2. O_2 became increasingly limiting with the increase in biofilm thickness in time. From Day 4 to Day 7, accumulation of H_2 resumed, this time due to increasing O_2 limitation in the thick biofilm, consequently restricting H_2 consumption. The modeled CO_2, as used in the experimental setup, never limited biofilm growth.

Developing a continuous process for biofilm harvest and regrowth

At a certain thickness, biofilm growth is hindered by mass transfer limitations (Figure 4), indicating the point at which biomass should be harvested and used directly as a product or as a substrate in a biorefinery process [43]. The developed method for controlled biofilm detachment is based on the generation of H_2 at the cathode surface through the application of a negative potential. A similar technique was used previously to remove biofilms from a stainless steel surface [44]. For this study, in preliminary abiotic tests, the initiation of visible H_2 bubble formation was detected by observing abrupt decreases in current density, along with the detection of H_2 bubbles using OCT imaging (data not shown). H_2 bubbles began to form at –550 mV versus SHE at the chosen process conditions (60°C, pH 4.0, graphite electrode).

H_2 bubbles formed beneath the biofilm, causing partial destruction of the biofilm structure (Figure S4 in the supplemental information online). To quantitatively evaluate the impact of H_2 bubbles on biofilm detachment, a series of experiments was conducted, gradually decreasing the potential from –0.8 V to –2.8 V. The aim was to screen different negative potentials to observe the point at which H_2 evolution would lead to sufficient biofilm detachment. The relative biovolume and substratum coverage were measured using OCT (Figure 5A). Between –1.0 and –1.4 V,

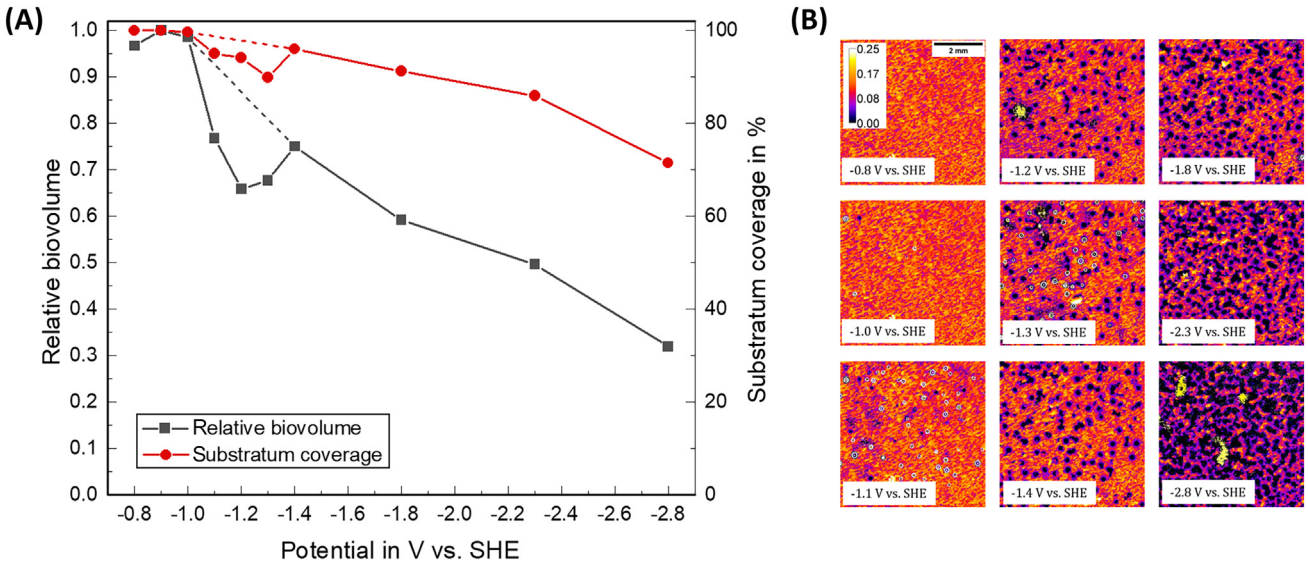

Figure 5. Harvesting the biofilm by applying negative potentials to the cathode. (A) Characterization of biofilm detachment by hydrogen bubbles with regards to relative biovolume and substratum coverage. Broken lines represent the presumed development of biovolume development, which was cumbersome to analyze due to hydrogen bubble localization. (B) Biofilm height profiles for decreasing negative potential; color calibration bar is given in mm. One experiment in which the potential was decreased stepwise for 2 min per step is shown. This experiment was representative of several biological replicates that were also conducted for each potential.

some residual bubbles cast shadows on the biofilm in the OCT images, leading to underestimation of biofilm measurements. These bubbles could not be removed due to their very small size. Therefore, the presumed more realistic development of biovolume and coverage in this area is depicted by broken lines in Figure 5.

Both the biovolume and substratum coverage exhibited an almost linear decrease with decreasing potential. The biovolume decreased by 65%, while the coverage of the cathode surface ultimately only decreased to 70%. For a visual impression of the harvesting process, please see Video S1 in the supplemental information online, which shows the harvesting process at a potential of −2.8 V.

Figure 4B displays the height profiles of the biofilm during the detachment steps. The height maps revealed H_2 bubble-induced voids within the biofilm, with an approximate radius of 300 µm, starting from −1.1 V versus SHE. As the potential decreased further, the number and size of these voids progressively increased.

To ensure the feasibility of a continuous process, it is important to demonstrate the ability of the biofilm to regenerate from the remaining cells located on or near the area of bubble formation on the cathode. To investigate this, the medium and all planktonic cells were replaced with fresh medium, and cultivation was restarted. The resulting biovolume and substratum coverage are presented in Figure 6A.

After detachment, 30% of the cathode surface was no longer covered by biofilm. Within the following 10 days, the growing biofilm completely covered the electrode surface again and regenerated to more than 70% of its initial volume before detachment (Figure 6B). The detached biomass was analyzed for its protein content, which was determined to be 62%. The amino acid composition of *K. spormannii* was analyzed using heterotrophically grown cells, revealing a molar

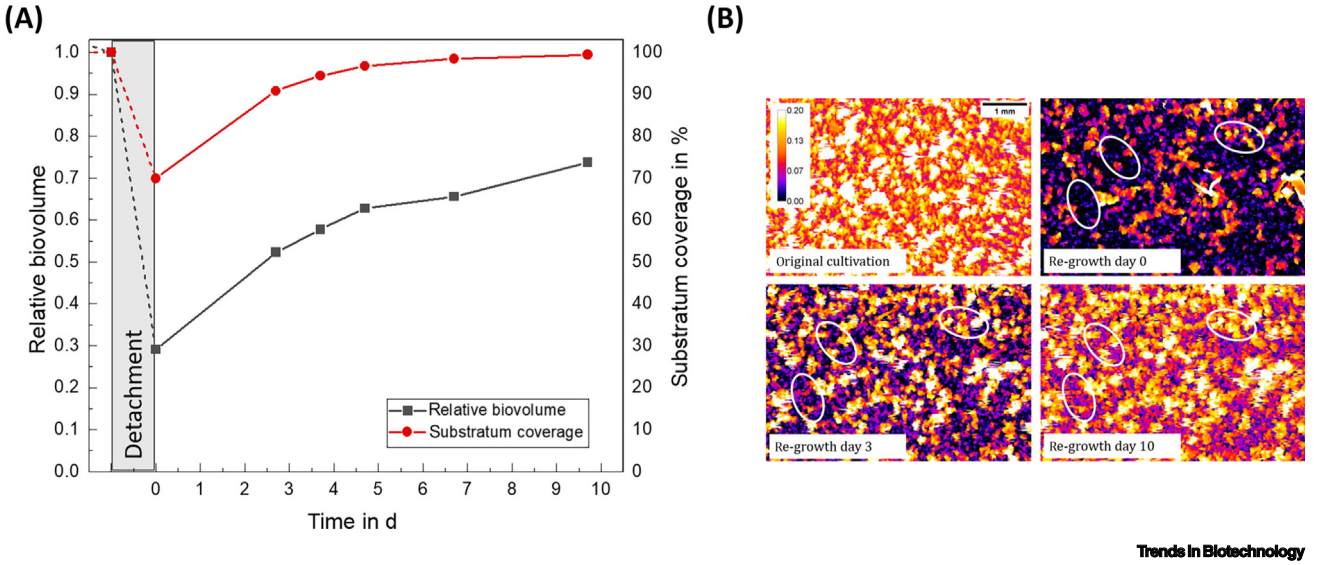

Figure 6. Biofilm regeneration after harvest. (A) Evolution of biovolume and substratum coverage in a harvested system without planktonic cells; (B) Height maps of the biofilm regrowing; color calibration bar is given in mm. Three positions are marked with white circles to allow for better assessment of biofilm regrowth. The two positions on the left in each image were completely uncovered in the beginning. On Day 10, spots were found that were re-covered with an ~0.07 mm-thick biofilm. The right marking in each image shows a small biofilm structure with a height of 0.1 mm at the start. On Day 10, it was 0.15 mm high. Hence, these images provide proof of regrowth of the biofilm in positions at which hydrogen bubbles caused the detachment of biofilm parts. Abbreviation: SHE, standard hydrogen electrode.

content of 41% of the nine essential amino acids that cannot be synthesized by mammals (histidine, isoleucine, leucine, lysine, methionine, phenylalanine, threonine, tryptophan, and valine) (Table S2 in the supplemental information online).

H_2/CO_2 ratio and electron efficiency for cathode- and knallgas-based growth

The theoretical H_2/CO_2 ratio for converting CO_2 into biomass is 2.1 mol mol^{-1}. This is because the carbon in CO_2 has an oxidation state of +4, which needs to be reduced to –0.2 in biomass. The electron demand for this process is described by the CE of CO_2 reduction to biomass (Figure 4A). However, the actual H_2/CO_2 ratio must be higher due to the catabolic H_2 consumption needed to generate enough ATP to allow the carbon of CO_2 to be integrated as biomass. The thermodynamic lower limit for the H_2/CO_2 ratio for autotrophic growth of the metabolically related organism *Cupriavidus necator* was calculated to be 2.4 mol H_2/mol CO_2 [45,46]. For *K. spormannii*, the actual H_2/CO_2 ratio was determined to be 7.5 mol mol^{-1}. Notably, for the closely related strain *Kyrpidia spormannnii* FAVT5, a recent paper revealed a similar efficiency of 7.14 mol mol^{-1} [47]. Achieving a similar electron efficiency in an OMES process compared with gas fermentation in a batch system is challenging because abiotic O_2 reduction at the cathode can act as a significant electron sink. The computational model developed for the OMES process was tuned by considering metabolic data from the litho-autotrophic growth of *K. spormannii* to adjust the experimental O_2 concentration according to the requirements of the organism and to avoid abiotic O_2 reduction as much as possible. The OMES process achieved a biotic electron consumption of up to almost 100% compared with the gas fermentation experiments conducted in bottles (Figure 4A). This related to a CE of 28%, because 72% of the electrons were used for catabolic purposes and did not aid directly in CO_2 reduction but rather in microbial energy generation via the respiratory chain. This calculation was based on the ratio of the theoretical to actual H_2/CO_2 demand of 0.28. Nevertheless, this demonstrates that even OMES can be operated with minor abiotic losses. During the period of maximum CE, the electrode was entirely covered with biofilm. On average, the CE reached 19.7%, while 28% was the achievable maximum, as mentioned

above. This lower value is due to the lag phase exhibiting lower efficiency compared with the exponential growth phase, likely because of abiotic O_2 reduction.

We used the established model to calculate concentration gradients of H_2 and O_2 across the developing biofilm for Days 2 and 5 of the experiment (Figure 4B). The average current density was utilized to model H_2 evolution. Notably, the average current density in this experiment was –65 μA cm^{-2}, which resulted from the generally higher O_2 concentration compared with the initial growth experiments conducted at –500 mV. During cultivation, the biofilm went through different growth regimes determined by the availability of the two substrates. In a relatively thin biofilm of ~100 μm (Day 2, Figure 4B), neither H_2 nor O_2 was growth limiting, because the substrates diffused through the whole biofilm thickness.

On Day 5, the biofilm was ~200 μm thick, and there was enough O_2 supplied from the bulk phase and H_2 counter-diffusing from the cathode, to sustain growth. At this stage, it was O_2 that started becoming limiting to the growth. This agreed well with the observed increase in CE from Day 2 to Day 5, because more O_2 was depleted by the biofilm and, therefore, could not serve as an electron sink for abiotic redox reactions. The carbon source (here CO_2) was always in excess under the applied conditions. The accuracy of the model is sufficient to explain the limitations that will hamper biofilm growth at different biovolumes and suggests that biofilm harvesting should occur at this point where growth rate and CE are in an optimal range.

Estimation of the energy demand of OMES

As one of the primary objectives of this process is to convert CO_2 into biomass, the solar energy required to generate a specific biomass quantity was calculated for the OMES process. Notably, the calculations were based on the bioelectrochemical flow cell system, which is optimal for the study conducted here, but at a low Technology Readiness Level (TRL). This proof-of-principle process was compared with phototrophic biomass production and biomass production based on *K. spormannii* growing on knallgas using electrolysis-produced H_2. For simplicity and to reach comparability, it was assumed that only the availability of electrons and energy for these electrons limited the productivity of the biosystems. In addition, values regarding the process periphery were not accounted for because this is not yet comparable due to the different TRLs and scales of the technologies. In other words, the analysis considered only the energy required to provide the electrons for the reduction of CO_2 into biomass, while overlooking the peripheral processes necessary to facilitate this conversion (pumping, heating, infrastructure, etc.). This simplification allowed for a comparison between technologies and OMES, even though some of these technologies have reached significantly higher TRLs.

The energy demand for the production of 1 kg dry biomass was calculated using the cell voltage multiplied by the integral of the electric current (see Equation 2 in the STAR★METHODS). In our study, the average conversion efficiencies from sunlight to biomass were assumed to be 1.5% for C_3 plants and 3.5% for C_4 plants, respectively (these values correspond to published data for plants in fields with sufficient nutrient and water supply during their active vegetation phase) [48]. The median solar energy demand for cathodic growth was calculated to be 204.57 kWh kg^{-1}. Of note, energy demand for the most efficient process window of the OMES would correspond to a solar energy demand of only 67.89 kWh kg^{-1}. This value could be reached if most of the biofilm community could be kept at the optimal growth rate that was reached between Days 4 and 5.

For knallgas bacteria, which utilize H_2 as an electron donor, there is also the option to produce H_2 in an external electrolyzer first, which can then be supplied to the bacteria in a second step. The

carbon content in dry biomass accounts for 48.8% of its weight [49]. With a theoretical H_2 demand of 2.1 mmol H_2 per mmol carbon, a final demand of 0.19 kg of H_2 kg^{-1} of dry biomass was assumed. The voltage efficiency for proton exchange membrane (PEM) electrolysis and alkaline electrolysis, for cell voltages of 1.8–2.24 V, is 62–82%. This leads to an energy demand of ~45–50 kWh kg^{-1} of H_2 [14,50]. Considering the photovoltaic conversion efficiency of 17.5%, this biomass production method results in a solar energy demand of 48.78 kWh kg^{-1} of dry biomass under optimal conditions. However, when considering the realistic values for H_2 efficiency determined in this study, the energy demand more than triples to 174.2 kWh kg^{-1} (Figure 7).

The OMES and knallgas-based processes were also compared with photosynthesis in C_3 and C_4 plants, as well as microalgae cultivation. A higher efficiency for a Knallgas-based bacterial biomass production compared with photosynthetic efficiency was reported by Lepidi and colleagues in 1990 [51]. The calorific value for a whole plant was determined to be 0.0175 MJ g^{-1} by Lieth and colleagues [52], resulting in a solar energy demand of 324.07 kWh kg^{-1} for C_3 plants or 138.89 kWh kg^{-1} for C_4 plants. Hence, OMES could result in competitive efficiencies (i.e., an exclusive consideration of the energy required in the conversion of radiation to biomass without upstream and downstream process steps). This is primarily due to the higher conversion efficiency of photovoltaic systems compared with photosynthesis [53,54]. The photo conversion efficiency (PCE), which describes the efficiency of sunlight conversion in a production system for microalgae, ranges between 1% (open pond cultivation) and 10% (theoretical maximum). For our calculation, a PCE of 5% was assumed, which would occur in a realistic outdoor reactor. Given that microalgae biomass has an energy content of 20 MJ kg^{-1} dry biomass, the resulting solar energy demand was 111.11 kWh kg^{-1} [55,56].

Discussion

Recently, Reiner and colleagues published a review addressing whether OMES could serve as a viable alternative for biomass production [57]. The authors acknowledged the potential of the process but highlighted several significant challenges that must be overcome, including the establishment of a complete mass balance, development of mathematical models, and identification of optimal process parameters [57]. The study presented here directly addresses these gaps and offers a methodological framework to tackle the associated challenges effectively.

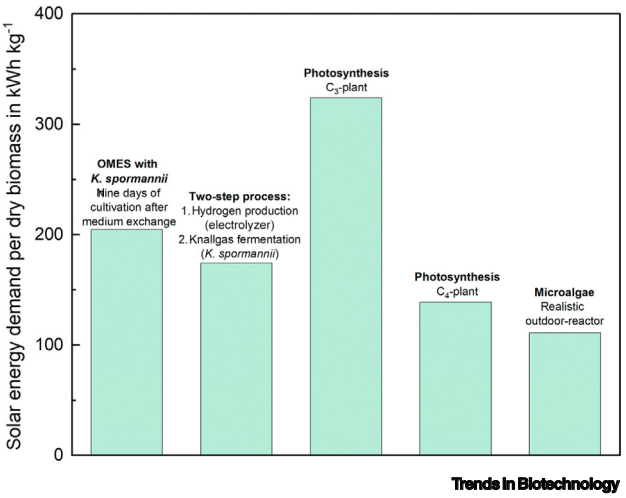

Figure 7. Solar energy demand for biomass-producing processes. Shown here is the solar energy demand for the production of 1 kg dry biomass with the cultivation of Kyrpidia *spormannii* in the described oxic microbial electrosynthesis (OMES) process at –500 mV (the whole cultivation period of 9 days is shown), the production of hydrogen for cultivation of knallgas *K. spormannii* in an external electrolyzer, photosynthesis in plants (C_3 and C_4 metabolism), and microalgae cultivation in a realistic outdoor reactor. The lower the solar energy demand per weight of biomass, the more energy efficient the accompanying process. The solar energy demand for OMES using *K. spormannii* was considerably lower after full coverage of the cathode surface and decreased to <68 kWh kg^{-1} dry biomass.

We established that oxic autotrophic cathode-based biomass production can be conducted in a continuous process with minor losses due to the abiotic interaction of O_2 with the electrode surface. Hence, future process development might lead to a competitive technology compared with other established processes. Along these lines, future biotechnological processes will at best have to operate continuously over long periods of time. If a process is supposed to be catalyzed by a single organism under axenic conditions, the risk of contamination is a tremendous problem. The more specific and extremophilic the conditions are, the lower the contamination risk. The extremophilic microbe used here fulfils the requirements for a process that lowers the risk for contamination by design. In preliminary experiments, we showed growth of *K. spormannii* using off-gas from companies from the waste burning and energy sector (data not shown). These substrates would necessitate cooling if the current model organisms for MES were used.

Adjusting O_2 concentration in correlation with biofilm coverage and growth will be key to establish the highest energy efficiency. This result agrees with end point analysis of a previous study for the same organism, which revealed that, within a O_2 concentration of 0.5–20% in the reservoir head space, optimal growth could be achieved with 2.5% O_2 and a cathode potential of –625 mV. The dissolved O_2 concentration and growth kinetics were not determined [39]. Regarding the cathode potential, we determined similar biofilm growth kinetics at –375 mV and –500 mV versus SHE. At 0 mV, we observed very slow and linear growth. Moreover, the accumulation rate was not affected by the cathode potential when comparing –375 mV and –500 mV. Notably, the time points of the maximum accumulation rate correlated with 50% of the maximum biovolume in the cultivations at –375 mV and –500 mV versus SHE. Our modeling approach allowed the assessment of the point at which access to O_2 most likely limited further biomass development during biofilm growth. Biofilm height represents a process-limiting parameter after which biofilm growth slows. A similar observation was made in a mathematical model of an MES process provided by Li and colleagues [58]. In general, mathematical modeling of OMES processes is an important tool for predicting biofilm growth and optimizing energy efficiency and productivity in terms of maximum biomass yield. The described model will be further optimized to serve as such a prediction tool. Variation in biofilm structure related to electrode potential was most probably due to inhomogeneous H_2 formation on the cathode surface correlated with lower electrode potentials. To this end, it would be interesting to observe how H_2 forms at different potentials and what the impact of very small H_2 bubbles might be on the process. Unfortunately, this was below the resolution limit of the analytic infrastructure and will be investigated in future work.

Mishra and colleagues calculated an energy demand of 29.24 kWh kg^{-1} biomass for H_2-oxidizing knallgas bacteria fed with externally produced H_2 [41]. More than 50% of the supplied electrons were utilized to reduce CO_2 to biomass. This value is significantly higher than the average anabolic H_2 utilization of acetogenic or methanogenic organisms, which is ~10%. Consequently, biomass production by these organisms carries a significantly higher energy demand due to a very low CO_2 to biomass conversion efficiency [59]. In fact, according to Mishra and colleagues, the energy demand for autotrophically grown acetate-producing bacteria is 231.48 kWh kg^{-1} biomass [41]. The rather high energy demand might also hamper production of products besides biomass, because biocatalyst regrowth might be a process limitation [54]. Nevertheless, if methane, short-chain carboxylic acids, or corresponding alcohols are the envisioned process products, methanogens and acetogens will be the organisms of choice, because these products are produced with high efficiency. Moreover, it will be possible to realize two-step processes in which the end products of the acetogenic primary producers are used by aerobic organisms for biomass growth. This process was suggested by Molitor and colleagues and led to a carbon

efficiency of the final yeast biomass of 25% [60]. Nevertheless, one-step cathodic biomass production will most likely be more efficient using *K. spormannii* and comparable organisms compared with acetogens or methanogens.

In terms of not only the share of supplied electrons ending up in biomass, but also the overall energy efficiency, it might be worth considering oxic cathodic processes for future biomass production, especially if the process can be kept within an optimum window of biofilm height and coverage. In this context, Reiner and colleagues compared heterotrophic, phototrophic, and lithoautotrophic approaches with biomass production [57]. Their calculations suggested that OMES would be competitive with many existing technologies regarding energy requirements. It was proposed that OMES might have only a slightly higher energy demand compared with established, upscaled technologies, such as Quorn, which is produced through the heterotrophic fermentation of organic carbon using the fungus *Fusarium venenatum* [61].

The described method of biofilm detachment not only allows for steering process efficiency, but also serves as a significant downstream processing step for biomass harvesting. In addition, downstream processing will benefit from the larger biofilm flocs that are harvested via bubble formation, because it will be easier to separate flocs than individual cells from the medium. To this end, regarding the current development of the global population, it appears inevitable to reconsider how protein for food and feed is produced. The process described here might be an option for this so-called 'protein transition', because analysis of the amino acid composition of the *K. spormannii* biomass revealed that it contains all essential amino acids, as expected; however, unlike plant biomass, the caloric value of this bacterial biomass is as yet unknown. However, there are several studies of the biomass composition of H_2-oxidizing bacteria. According to Volova and Barashkov, the protein content synthesized by H_2-oxidizing bacteria in a two-step process can be up to 70% of the cell dry weight [62]. Furthermore, the biological values of these proteins were found to be similar to those produced by animals or plants. Additionally, Pous and colleagues showed that protein rich biomass with a protein content of up to 64% of dry cell weight can also be obtained in an OMES process [37]. The protein content of 62% determined here correlates well with their study. Of note, the overall amino acid content is also similar to research conducted with yeast cells [63]. Given that it cannot be expected that the *K. spormannii* biomass will differ significantly compared with other single cell protein sources, we expect that its biomass will also be a valuable vitamin source [64].

Although the results of this study are encouraging for the further development of an OMES process, this development poses a major challenge. So far, there is no established, scalable reactor technology for this process that would allow the biomass to be trimmed to an optimal height while adjusting the dissolved O_2 concentration according to the biofilm height. It would also be desirable to run the process at atmospheric CO_2 concentrations, but this has not yet been tested. Nevertheless, we have performed growth experiments with *K. spormannii* using hot exhaust gas from CO_2 point sources, such as waste incinerators, which showed the same or similar growth characteristics compared with bottled gases. Furthermore, it would be desirable to have a genetic system for *K. spormannii* that would not only allow the reprogramming of metabolism toward the production of other valuable end products besides biomass, but also a basic understanding of the fundamentals of microbe–electrode interactions. While rapid growth appears to be dependent on H_2 evolution, we also observed growth at higher electrode potentials, which are unlikely to be sufficient for electrochemical H_2 production. If parallel electron import and usage strategies exist, it might be possible to develop the organism for better growth at higher potentials, which would increase energy efficiency considerably.

Concluding remarks

According to Prévoteau and colleagues [54], challenges for MES predominantly include nonselective production at low product titers, low production rates, high cell voltage (ohmic drop) resulting in low energy conversion efficiency, and high capital costs. With OMES some of these aspects could be overcome, although a higher TRL has to be achieved to gain more quantitative data. Our findings demonstrate that a cathode potential between –375 mV and –500 mV versus SHE can lead to rapid biofilm growth. By applying a highly negative potential, we propose a method for partially harvesting the biofilm by generating H_2 bubbles. The biofilm can regenerate after partial harvesting, enabling continuous operation of the process. The CE for biobased electron usage reaches up to 100% at its maximum. Moreover, oxic cathodic processes eliminate the need for a membrane to separate the anode and cathode, resulting in a substantial decrease in capital costs, because membranes typically constitute the most expensive component of bioelectrochemical systems. Thus, the potential of OMES should not be underestimated.

We do not as yet have a clear path toward a reliable storage system for electrical energy. The technology described here so far stores energy in the form of biomass, which could be seen as an alternative and resource-efficient farming technology. Moreover, genetic engineering of the organism will allow for the production of a broad spectrum of end products that could include either easily usable energy carriers directly or platform chemicals that could later be chemically converted to, for instance, liquid energy carriers. Nevertheless, a complete technoeconomic analysis will be necessary to fully compare OMES with other technologies and to calculate the costs that would be required for industrial realization. This will require future studies on scalable reactor systems to provide robust numbers for potential capital expenditures (see Outstanding questions). This scalable reactor system will also be necessary to study whether volumetric production rates can be competitive, which is one of the major hurdles mentioned by Prévoteau and colleagues [54].

Outstanding questions

Is the metabolism of *Kyrpidia spormannii* thriving on electrodes only based on H_2 evolution at the cathode or are there parallel ways of electron import into the respiratory chain?

How can electron losses and potential formation of reactive oxygen species be limited during incomplete coverage of the electrode by *K. spormannii* ?

What would be suitable reactor architectures for upscaling of the technology?

Can we further increase the productivity of the system by adjusting process conditions and laboratory evolution of the organisms?

Can we apply the same process strategy with similar results to other aerobic hydrogenotrophic organisms?

STAR★METHODS

Detailed methods are provided in the online version of this paper and include the following:

- KEY RESOURCES TABLE
- EXPERIMENTAL MODEL AND STUDY PARTICIPANT DETAILS
- METHOD DETAILS
  - Harvesting the biofilm, determining protein concentration and amino acid composition
  - Optical coherence tomography (OCT) and image processing
  - Quantifying the density of the dry biofilm
  - Determination of H_2/CO_2 ratio for autotrophic growth of *K. spormannii*
  - Calculation of coulombic efficiency (CE) and energy demand
  - Numerical model of *Kyrpidia spormannii* biofilm
    - Phases and geometry
    - The biofilm
    - Biofilm thickness
    - Bulk liquid
    - Gas phase
    - Solution method
    - Parameters
  - Thermodynamic derivation of microbial stoichiometry
    - Catabolic reaction
    - Anabolic reaction

RESOURCE AVAILABILITY

Lead contact

Requests for further information and resources should be directed to and will be fulfilled by the lead contact, Johannes Gescher (johannes.gescher@tuhh.de).

Materials availability

This study did not generate new unique reagents.

Data and code availability

All data reported in this article, as well as the described model, will be shared by the lead contact upon request. This article does not report original code. Any additional information required to re-analyze the data reported in this paper is available from the lead contact upon request.

Acknowledgments

This work was supported by a grant of the Bundesministerium für Bildung und Forschung (BMBF), no. 033RC006.

Declaration of interests

None declared by authors.

Supplemental information

Supplemental information to this article can be found online at https://doi.org/10.1016/j.tibtech.2024.11.005.

References

1. Hofmann, D.J. *et al.* (2006) The role of carbon dioxide in climate forcing from 1979 to 2004: Introduction of the Annual Greenhouse Gas Index. *Tellus B* 58, 614–619
2. Falkowski, P. *et al.* (2000) The global carbon cycle: a test of our knowledge of earth as a system. *Science* 290, 291–296
3. Friedlingstein, P. (2015) Carbon cycle feedbacks and future climate change. *Philos. Trans. R. Soc. A Math. Phys. Eng. Sci.* 373, 20140421
4. Dixon, R.K. and Turner, D.P. (1991) The global carbon cycle and climate change: Responses and feedbacks from below-ground systems. *Environ. Pollut.* 73, 245–262
5. Fischer, F. and Tropsch, H. (1927) Über die Synthese hochmolekularer Paraffin-Kohlenwasserstoffe aus Kohlenoxyd. *Ber. Dtsch. Chem. Ges.* 60, 1330–1334
6. Inderwildi, O.R. *et al.* (2008) Fischer-Tropsch mechanism revisited: alternative pathways for the production of higher hydrocarbons from synthesis gas. *J. Phys. Chem. C* 112, 1305–1307
7. Mota, F.M. and Kim, D.H. (2019) From CO2 methanation to ambitious long-chain hydrocarbons: Alternative fuels paving the path to sustainability. *Chem. Soc. Rev.* 48, 205–259
8. Schmid, A. *et al.* (2001) Industrial biocatalysis today and tomorrow. *Nature* 409, 258–268
9. Rabaey, K. *et al.* (2011) Metabolic and practical considerations on microbial electrosynthesis. *Curr. Opin. Biotechnol.* 22, 371–377
10. Chen, H. *et al.* (2020) The progress and outlook of bioelectrocatalysis for the production of chemicals, fuels and materials. *Nat. Catal.* 3, 225–244
11. Rosenbaum, M.A. *et al.* (2013) Mikroben unter Strom. *Biol. Zeit.* 2013, 96–103
12. Berg, I.A. (2011) Ecological aspects of the distribution of different autotrophic CO2 fixation pathways. *Appl. Environ. Microbiol.* 77, 1925–1936
13. Kracke, F. *et al.* (2015) Microbial electron transport and energy conservation - the foundation for optimizing bioelectrochemical systems. *Front. Microbiol.* 6, 575
14. Carmo, M. *et al.* (2013) A comprehensive review on PEM water electrolysis. *Int. J. Hydrog. Energy* 38, 4901–4934
15. Tan, X. and Nielsen, J. (2022) The integration of bio-catalysis and electrocatalysis to produce fuels and chemicals from carbon dioxide. *Chem. Soc. Rev.* 51, 4763–4785
16. Elisiário, M.P. *et al.* (2022) Membrane bioreactors for syngas permeation and fermentation. *Crit. Rev. Biotechnol.* 42, 856–872
17. Bian, B. *et al.* (2020) Microbial electrosynthesis from CO2 : challenges, opportunities and perspectives in the context of circular bioeconomy. *Bioresour. Technol.* 302, 122863
18. Choi, O. and Sang, B.I. (2016) Extracellular electron transfer from cathode to microbes: application for biofuel production. *Biotechnol. Biofuels* 9, 11
19. Reiner, J.E. *et al.* (2020) From an extremophilic community to an electroautotrophic production strain: identifying a novel Knallgas bacterium as cathodic biofilm biocatalyst. *ISME J.* 14, 1125–1140
20. Jung, T. *et al.* (2021) Improving the cathodic biofilm growth capabilities of *Kyrpidia spormannii* EA-1 by undirected mutagenesis. *Microorganisms* 9, 77
21. Halan, B. *et al.* (2012) Biofilms as living catalysts in continuous chemical syntheses. *Trends Biotechnol.* 30, 453–465
22. Izadi, P. *et al.* (2020) Parameters influencing the development of highly conductive and efficient biofilm during microbial electrosynthesis: the importance of applied potential and inorganic carbon source. *Biofilms Microbiomes* 6, 40
23. Jourdin, L. *et al.* (2016) Biologically induced hydrogen production drives high rate/high efficiency microbial electrosynthesis of acetate from carbon dioxide. *ChemElectroChem* 3, 581–591
24. Cabau-Peinado, O. *et al.* (2024) Microbial electrosynthesis from CO2 reaches productivity of syngas and chain elongation fermentations. *Trends Biotechnol.*, Published online August 8, 2024. https://doi.org/10.1016/j.tibtech.2024.06.005
25. Mayer, F. *et al.* (2019) Performance of different methanogenic species for the microbial electrosynthesis of methane from carbon dioxide. *Bioresour. Technol.* 289, 121706
26. Kracke, F. *et al.* (2020) In situ electrochemical H2 production for efficient and stable power-to-gas electromethanogenesis. *Green Chem.* 22, 6194–6203
27. Kracke, F. *et al.* (2021) Efficient hydrogen delivery for microbial electrosynthesis via 3D-printed cathodes. *Front. Microbiol.* 12, 696473
28. Ning, X. *et al.* (2021) Emerging bioelectrochemical technologies for biogas production and upgrading in cascading circular bioenergy systems. *iScience* 24, 102998
29. Nevin, K.P. *et al.* (2011) Electrosynthesis of organic compounds from carbon dioxide is catalyzed by a diversity of acetogenic microorganisms. *Appl. Environ. Microbiol.* 77, 2882–2886
30. Ganigué, R. *et al.* (2015) Microbial electrosynthesis of butyrate from carbon dioxide. *Chem. Commun.* 51, 3235–3238
31. Vassilev, I. *et al.* (2018) Microbial electrosynthesis of isobutyric, butyric, caproic acids, and corresponding alcohols from carbon dioxide. *ACS Sustain. Chem. Eng.* 6, 8485–8493
32. Dessì, P. *et al.* (2021) Microbial electrosynthesis: towards sustainable biorefineries for production of green chemicals from CO2 emissions. *Biotechnol. Adv.* 46, 107675
33. Boto, S.T. *et al.* (2023) Microbial electrosynthesis with *Clostridium ljungdahlii* benefits from hydrogen electron mediation and permits a greater variety of products. *Green Chem.* 25, 4375–4386
34. Salehizadeh, H. *et al.* (2020) Recent advances in microbial CO2 fixation and conversion to value-added products. *Chem. Eng. J.* 390, 124584

35. Bar-Even, A. *et al.* (2012) A survey of carbon fixation pathways through a quantitative lens. *J. Exp. Bot.* 63, 2325–2342
36. Jajesniak, P. *et al.* (2014) Carbon dioxide capture and utilization using biological systems: opportunities and challenges. *J. Bioprocess. Biotech.* 4, 3
37. Pous, N. *et al.* (2022) Electro-cultivation of hydrogen-oxidizing bacteria to accumulate ammonium and carbon dioxide into protein-rich biomass. *Bioresour. Technol. Reports* 18, 101010
38. Langsdorf, A. *et al.* (2024) Production of polyhydroxybutyrate from industrial flue gas by microbial electrosynthesis. *J. CO2 Util.* 83, 102800
39. Pillot, G. *et al.* (2022) Optimization of growth and electrosynthesis of polyhydroxyalkanoates by the thermophilic bacterium *Kyrpidia spormannii*. *Bioresour. Technol. Reports* 17, 100949
40. Marcellin, E. *et al.* (2022) Recycling carbon for sustainable protein production using gas fermentation. *Curr. Opin. Biotechnol.* 76, 102723
41. Mishra, A. *et al.* (2020) Power-to-protein: carbon fixation with renewable electric power to feed the world. *Joule* 4, 1142–1147
42. Reiner, J.E. *et al.* (2018) *Kyrpidia spormannii* sp. nov., a thermophilic, hydrogenoxidizing, facultative autotroph, isolated from hydrothermal systems at São Miguel Island, and emended description of the genus *Kyrpidia*. *Int. J. Syst. Evol. Microbiol.* 68, 3735–3740
43. Vassilev, I. *et al.* (2022) Cathodic biofilms – a prerequisite for microbial electrosynthesis. *Bioresour. Technol.* 348, 126788
44. Wijesinghe, M.S. *et al.* (2018) Demonstration of biofilm removal from type 304 stainless steel using pulsed-waveform electropolishing. *Biofouling* 34, 731–739
45. Yu, J. *et al.* (2013) The energy efficiency of carbon dioxide fixation by a hydrogen-oxidizing bacterium. *Int. J. Hydrog. Energy* 38, 8683–8690
46. Lu, Y. and Yu, J. (2017) Comparison analysis on the energy efficiencies and biomass yields in microbial CO2 fixation. *Process Biochem.* 62, 151–160
47. Hogendoorn, C. *et al.* (2020) Hydrogen and carbon monoxide-utilizing *Kyrpidia spormannii* species from *Pantelleria*. *Front. Microbiol.* 11, 951
48. Éva, C. *et al.* (2019) Current and possible approaches for improving photosynthetic efficiency. *Plant Sci.* 280, 433–440
49. Heijnen, J.J. and Kleerebezem, R. (2010) Bioenergetics of microbial growth. In *Encyclopedia of Industrial Biotechnology: Bioprocess, Bioseparation, and Cell Technology* (Flickinger, M.C., ed.), Wiley. https://doi.org/10.1002/9780470054581.eib084
50. Chen, Y.X. *et al.* (2014) Nanotechnology makes biomass electrolysis more energy efficient than water electrolysis. *Nat. Commun.* 5, 4036
51. Lepidi, A.A. *et al.* (1990) Hydrogen-oxidizing bacteria for biomass production. *Int. J. Hydrog. Energy* 15, 485–489
52. Lieth, H. (1975) Measurement of caloric values. In *Primary Productivity of the Biosphere* (Lieth, H. and Whittaker, R.H., eds), pp. 119–129, Springer
53. Blankenship, R.E. *et al.* (2011) Comparing photosynthetic and photovoltaic efficiencies and recognizing the potential for improvement. *Science* 332, 805–809
54. Prévoteau, A. *et al.* (2020) Microbial electrosynthesis from CO2: forever a promise? *Curr. Opin. Biotechnol.* 62, 48–57
55. Kaltschmitt, M. *et al.* (2016) Aquatische Biomasse. In *Energie aus Biomasse: Grundlagen, Techniken und Verfahren* (3rd edn) (Kaltschmitt, M. *et al.*, eds), pp. 249–277, Hofbauer, Hermann
56. Wilhelm, C. *et al.* (2014) Conversion steps in bioenergy production - analysis of the energy flow from photon to biofuel. *Biofuels* 5, 385–404
57. Reiner, J.E. *et al.* (2024) Oxygen in the mix: is oxic microbial electrosynthesis a potential alternative for biomass production? *ChemElectroChem* 11, e202400397
58. Li, W. *et al.* (2022) Simulation of cathode for synthesizing organic acids by MES reduction of CO2. *Bioelectrochemistry* 143, 107984
59. LaBelle, E.V. and May, H.D. (2017) Energy efficiency and productivity enhancement of microbial electrosynthesis of acetate. *Front. Microbiol.* 8, 756
60. Molitor, B. *et al.* (2019) Power-to-protein: converting renewable electric power and carbon dioxide into single cell protein with a two-stage bioprocess. *Energy Environ. Sci.* 12, 3515–3521
61. Wiebe, M.G. (2004) QuornTM Myco-protein - overview of a successful fungal product. *Mycologist* 18, 17–20
62. Volova, T.G. and Barashkov, V.A. (2010) Characteristics of proteins synthesized by hydrogen-oxidizing microorganisms. *Appl. Biochem. Microbiol.* 46, 574–579
63. Aruna, T.E. *et al.* (2017) Protein enrichment of yam peels by fermentation with *Saccharomyces cerevisiae* (BY4743). *Ann. Agric. Sci.* 62, 33–37
64. Sharif, M. *et al.* (2021) Single cell protein: sources, mechanism of production, nutritional value and its uses in aquaculture nutrition. *Aquaculture* 531, 735885
65. Hackbarth, M. *et al.* (2020) Monitoring and quantification of bioelectrochemical *Kyrpidia spormannii* biofilm development in a novel flow cell setup. *Chem. Eng. J.* 390, 124604
66. Bradford, M. (1976) A rapid and sensitive method for the quantitation of microgram quantities of protein utilizing the principle of protein-dye binding. *Anal. Biochem.* 72, 248–254
67. Wagner, M. and Horn, H. (2017) Optical coherence tomography in biofilm research: a comprehensive review. *Biotechnol. Bioeng.* 114, 1386–1402
68. Bauer, A. *et al.* (2019) In-situ monitoring and quantification of fouling development in membrane distillation by means of optical coherence tomography. *J. Membr. Sci.* 577, 145–152
69. Morinaga, Y. *et al.* (1978) Growth characteristics and cell composition of *Alcaligenes eutrophus* in chemostat culture. *Agric. Biol. Chem.* 42, 439–444
70. Bongers, L. (1970) Yields of *Hydrogenomonas eutropha* from growth on succinate and fumarate. *J. Bacteriol.* 102, 598–599
71. Mohammadi, S. *et al.* (2017) *Methylacidiphilum fumariolicum* SolV, a thermoacidophilic 'Knallgas' methanotroph with both an oxygen-sensitive and -insensitive hydrogenase. *ISME J.* 11, 945–958
72. Das, S. and Ghangrekar, M.M. (2018) Value added product recovery and carbon dioxide sequestration from biogas using microbial electrosynthesis. *Indian J. Exp. Biol.* 56, 470–478
73. IWA Task Group on Biofilm Modeling (2006) *Mathematical Modeling of Biofilms*, IWA Publishing

STAR★METHODS

KEY RESOURCES TABLE

Reagent or resource	Source	Identifier
Bacterial and virus strains		
Kyrpidia spormannii EA[1]	The strain was isolated from environmental samples in our lab	DSM 106492
Chemicals, peptides, and recombinant proteins		
Yeast extract	Roth	CAS: 8013-01-2
Peptone	Roth	CAS: 91079-40-2
Sodium pyruvate	Roth	CAS: 113-24-6
Casein hydrolysate	Roth	CAS: 65072-00-6
Soluble starch	Roth	CAS: 9005-25-8
K_2HPO_4	Roth	CAS: 7758-11-4
MOPS-buffer	Roth	CAS: 1132-61-2
H_2SO_4	Roth	CAS: 7664-93-9
NH4Cl	Roth	CAS: 12125-02-9
NaCl	Roth	CAS: 7647-14-5
KH2PO4	Roth	CAS: 7778-77-0
CaCl2	Roth	CAS: 10043-52-4
MgSO4 x 7H2O	Roth	CAS: 10034-99-8
MnSO4 x H2O	Roth	CAS: 10034-96-5
FeSO4 x 7 H2O	Roth	CAS: 7782-63-0
CoCl2 x 6 H2O	VWR Chemicals	CAS: 7791-13-1
CaCl2 x 2 H2O	Roth	CAS: 10035-04-8
ZnSO4 x H2O	Merck	CAS: 7446-19-7
CuSO4 x 5 H2O	Merck	CAS: 7758-99-8
KAl(So4)2 x 12 H2O	Roth	CAS: 7784-24-9
H3BO3	Merck	CAS: 10043-35-3
Na2MoO4 x 2H2O	Sigma Aldrich	CAS: 10102-40-6
H8N2NiO8S2 x 6 H2O	FLUKA Chemicals	CAS: 7785-20-8
Na2O4W x 2H2O	VWR Chemicals	CAS: 10213-10-2
Na2SeO4	Acro Organics	CAS: 13410-01-0
Software and algorithms		
Comsol model	Built for this study	N/A
Other		
Mass flow controller (gas)	Bronkhorst (NL)	EL-FLOW Select
Potentiostat	Gamry Instruments, Warminster (USA)	Gamry Interface 1010
Ag/AgCl reference electrode	Sensortechnik Meinsberg, Waldheim (GER)	SE23I
TOC analyzer	Analytik Jena, Jena (GER)	Multi N/C 2100 S
Optical Coherence Tomography	Thorlabs, Dachau (GER)	Ganymede, LSM03 lens
MikroGC	Agilent Technologies, Waldbronn (GER)	MikroGC 490

EXPERIMENTAL MODEL AND STUDY PARTICIPANT DETAILS

Heterotrophic *K. spormannii* pre-cultures were cultivated in modified R2A-Medium (5 g l^{-1} yeast extract, 1 g l^{-1} peptone, 1 g l^{-1} sodium pyruvate, 0.5 g l^{-1} casein hydrolysate, 0.5 g l^{-1} soluble starch, 0.1 g l^{-1} K_2HPO_4, 10 mM MOPS-buffer; pH set to 6.0 with 1 M H_2SO_4) at a temperature of 60°C. ES minimal medium (0.53 g l^{-1} NH_4Cl, 0.15 g l^{-1} NaCl, 0.04 g l^{-1} KH_2PO_4, 0.12 ml l^{-1} $MgSO_4$ (1 M), 1 ml l^{-1} $CaCl_2$ (0.1 M), 1 ml l^{-1} Wolfe's mineral elixir; pH 4.0) was used for all electroautotrophic cultivations. The heterotrophically-grown pre-cultures were washed in ES medium twice before they were used for inoculating the bioelectrochemical system (BES). A recently described flow cell system was used for bioelectrochemical experiments [65] (Figure S1 in the supplemental information online). Here, a smooth graphite plate was used as a cathode while iridium-tantalum coated titanium was used for the counter electrode. The smooth graphite plate was used in order to simplify biomass quantification. For the carbon supply, a CO_2-enriched medium was pumped from a stainless steel vessel to the biofilms in the flow cell with a flow rate of 100 ml min^{-1}. The vessel headspace of 150 ml was pressurized to 1.5 bar overpressure. The system was operated in batch mode. The gas phase was changed every one to three days or according to oxygen demand using a mixture of oxygen (2%–10%) and carbon dioxide (90–98%) produced using mass flow controllers (Gasmischer EL-FLOW; Bronkhorst, The Netherlands). The medium was continuously stirred and heated to 60°C.

The cathode served as the sole energy and electron (hydrogen) donor for the organisms. The electrical energy input was regulated using chronoamperometry. A Gamry Interface 1010 potentiostat (Gamry Instruments, Warminster, USA) was employed for potential control. The potential was applied relative to a Ag/AgCl reference electrode (SE23I, Sensortechnik Meinsberg, Waldheim, Germany). The potential was adjusted according to an internal resistance correction between the working and reference electrodes. This manuscript references the potential of the standard hydrogen electrode (SHE; 0 mV versus SHE corresponds to +199 mV versus Ag/AgCl). A cyclic voltammogram taken from the abiotic setup between 0 mV and −750 mV versus SHE was added to the supplementary part of the manuscript (Figure S2 in the supplemental information online). Please note that the bioelectrochemical experiments were conducted at pH 4 and that the redox potential for proton reduction to hydrogen will increase by 59 mV per pH unit compared with the potential of −413 mV at pH 7.

METHOD DETAILS

Harvesting the biofilm, determining protein concentration and amino acid composition

The biofilms were detached from the electrode surface by applying a two-minute potential pulse ranging from −0.8 V to −2.8 V versus SHE. This process induced the formation of macroscopic hydrogen bubbles between the cathode surface and the biofilm, leading to the detachment of the biofilm. The detached biomass was subsequently collected from the medium (see details below). If cultivation was to be continued, the entire medium was replaced with fresh, abiotic ES medium before resuming chronoamperometry. The protein content of the biomass was quantified using Bradford analysis [66]. Normalization to biomass was achieved by measuring the overall amount of organic carbon in the samples using a TOC analyzer (Multi N/C 2100 S; Analytik Jena, Jena, Germany), calculating back to biomass using the formula $CH_{1.8}N_{0.2}O_{0.5}$. Heterotrophically grown biomass was used to study its amino acid composition. The analysis was conducted at Alta Biosciences (UK) using acid protein hydrolysis and following chromatographic separation of the amino acids.

Optical coherence tomography (OCT) and image processing

The development of the biofilm was monitored using OCT with a Ganymede device equipped with an LSM03 lens (Thorlabs, Dachau, Germany). To ensure consistency and minimize the impact of flow effects on the imaging process, all images were taken at a fixed position in the center of the cathode [65].

A total area of 6 mm × 4 mm was scanned to obtain three-dimensional images. In order to facilitate comparison with other cultivation systems, the normalized biovolume was defined as the volume per unit area ($\mu m^3\ \mu m^{-2}$) [67]. By deriving the biovolume over time, the accumulation rate ($mm^3\ d^{-1}$ or $\mu m^3\ \mu m^{-2}\ d^{-1}$) could be determined. Processing of OCT images was conducted with ImageJ [65,68]. In addition to biovolume and accumulation rate, the substratum coverage and roughness coefficient were used as additional biofilm characteristics [67]. Biofilm porosity was calculated by subtracting the normalized biovolume from the mean height and then dividing the result by the mean height. According to a previous publication, we imaged individual spots which represent on average the biovolume of the whole cathode [65].

Quantifying the density of the dry biofilm

For energy efficiency calculations, the biovolume was converted into biomass. This conversion involved determining the density of the dry biofilm (ρ_{DBM}). To achieve this, the detached portions of the biofilm obtained after harvesting were collected by passing the medium through a sterile filter. Subsequently, the filter was dried for at least 4 days at 70°C. By measuring the difference in weight before and after drying, the weight of the harvested dry biomass (DBM) could be determined. Establishing a correlation between the difference in biovolume before and after the harvest from triplicate experiments enabled the establishment of a conversion factor of 30.4 ± 2.1 μg mm^{-3}.

Determination of H_2/CO_2 ratio for autotrophic growth of *K. spormannii*

In addition to carbon fixation, microbial electron consumption involves catabolic processes. To determine the actual electron demand of *K. spormannii*, the H_2/CO_2 ratio was measured during autotrophic growth. The experiments were conducted in bottles with defined a head space gas composition of 70% H_2, 20% CO_2, and 10% O_2. Gas concentrations were adjusted using three gas mass flow controllers (Bronkhorst, The Netherlands). The gas composition was measured at the beginning and end of the cultivation using a MicroGC 490 (Agilent Technologies). The bottles were incubated upside down to reduce the risk of hydrogen losses through the rubber stoppers. The consumption of H_2 and CO_2 was determined based on the difference in concentration. A ratio of 7.50 mol H_2 (mol CO_2)$^{-1}$ was calculated. The corresponding electron efficiency for CO_2 fixation, which is 28.0%, falls within the range of values determined for knallgas bacteria (*C. necator* 46.21% [69], *H. eutropha* 50.22% [70], *M. fumariolicum SolV* 34.15% [71]).

Calculation of coulombic efficiency (CE) and energy demand

The accumulated CE was calculated according to (t in days):

$$CE\ (t) = \frac{BV(t) \times \rho_{DBM} \times n_{e^-_{DBM}} \times F}{\int_0^t I(t)dt \times \tilde{M}_{DBM}} \times 100\%\ \ in\% \qquad [1]$$

The numerator represents the number of electrons required to form the cumulated biovolume during cultivation. BV(t) represents the absolute biovolume development (mm^3) over time. Using the density ρ_{DBM}, the biovolume can be converted into dry biomass, and by division by $\tilde{M}_{DBM}$ = 22.4 g mol^{-1}, the grown biomass in mol can be obtained. The amount of electrons needed to form 1 mol of dry biomass ($n_{e^-_{DBM}}$) was determined. In this calculation, biomass was assumed to have a composition of $CH_{1.8}N_{0.2}O_{0.5}$ (according to [49]), corresponding to a carbon oxidation state of –0.2. In CO_2, carbon has an oxidation state of +4. Thus, in theory and excluding catabolism, 4.2 mol of electrons are required to fix 1 mol of CO_2. Based on the H_2/CO_2 consumption ratio of the organism during autotrophic growth with hydrogen as the electron donor and energy source, the actual electron demand ($n_{e^-,\ DBM}$) was calculated to be 15 mol of electrons per mol of CO_2 (from the measured H_2 consumption). The denominator involves calculating the total number of supplied electrons over the observed time period. This is achieved by dividing the integral of the supplied electric current I(t) by the elementary charge e, which is included in the Faraday constant F (96 485 C mol^{-1}). The fraction is simplified accordingly.

Therefore, the CE at a certain time point includes all the biomass that has been built up from all the electrons that have been delivered since the beginning of the cultivation. The calculation was modified according to Das and Ghangrekar, who calculated the CE for their product acetate [72].

To prevent the inclusion of cells from the pre-culture that may falsely appear as autotrophically grown in the system, the medium was replaced with fresh anaerobic ES medium after one day, once the biofilm initiation occurred. This approach ensured that each subsequent increase in biovolume originated solely from cells grown within the system and not from the initial inoculum.

In addition to CE, the energy efficiency of a process was also characterized by the biomass yield per supplied energy. For simplicity and to enable the comparison of the value with other technologies, we only accounted here for the direct electrical energy used for biomass production. The supplied electrical energy was calculated by integrating the electrical input over

time. The electrical power was determined by multiplying the electrical current by the average cell voltage ($\overline{U}_{cell}$) of 1751 mV.

$$energy\ demand = \frac{\overline{U}_{cell} \times \int_0^t I(t)\,dt}{BV(t-t_0) \times \rho_{DBM}} \quad in \quad kWh\ (kg)^{-1} \qquad [2]$$

Numerical model of *Kyrpidia spormannii* biofilm

Phases and geometry. A mathematical model was constructed to represent and understand the observed trends in the biofilm growth by integrating physical/chemical/biological phenomena in a numerical framework. The time-dependent model represents 1D solute concentration gradients in growing biofilm, which are connected with concentration changes in the ideally-mixed aqueous phase; and associated with the changes in gas phase composition in the reactor headspace.

The biofilm. The model considered a planar biofilm varying in one dimension (variable thickness L_f) connected to the bulk water through mass transfer boundary layer ('diffusion boundary layer') with a fixed-thickness, L_{BL}. It was assumed that the biofilm is made of a pure culture of *K. spormannii* with constant biomass concentration c_X (C mol/m^3). Dissolved O_2 and H_2 were considered to be energy-supplying substrates and CO_2 was regarded as the carbon source. Molar concentrations of the three solutes c_i ($i = O_2, H_2, CO_2$) within the biofilm were found by solving the diffusion-reaction equation 3, with only diffusion in the mass transfer boundary layer ($r_i = 0$):

$$\frac{\partial c_i}{\partial t} = D_{i,F}\frac{\partial^2 c_i}{\partial x^2} + r_i \qquad [3]$$

Values of diffusion coefficients in the biofilm $D_{i,F}$ were reduced by a factor of f_{dif} from those in pure water D_i (at 60 °C), accounting for slightly hindered transport. The growth rate r_X was assumed as triple Monod limitation by O_2 (e-acceptor), H_2 (e-donor), and CO_2 (C-source, supplied in large excess from the gas phase):

$$r_X = \mu_m c_X \frac{c_{H_2}}{K_{H_2} + c_{H_2}} \frac{c_{O_2}}{K_{O_2} + c_{O_2}} \frac{c_{CO_2}}{K_{CO_2} + c_{CO_2}} \qquad [4]$$

Net rates r_i were linked stoichiometrically with the biomass growth rate:

$$r_{O_2} = -Y_{OX} r_X, r_{H_2} = -Y_{HX} r_X, r_{CO_2} = -Y_{CX} r_X \qquad [5]$$

The biomass specific growth rate is μ_m (1/d), half-saturation coefficients are K_{O2}, K_{H2}, K_{CO2} (mol/m^3) and yields are Y_{OX}, Y_{HX}, Y_{CX} (mol *i* / C mol biomass). At the biofilm base (x=0), a H_2 flux was set according to the mean current density i_{curr} (A/m^2) measured over the first 7 days of the biotic experiment, $r_{H_2,evol} = i_{curr}/(2F)$ (F =96485 C/mol), and O_2 and CO_2 fluxes were set to zero. Flux and concentration continuity were assumed at the biofilm surface in contact with water (x=L_F). At the boundary layer / bulk liquid boundary ($x = L_F + L_{BL}$), the concentrations in the liquid phase $c_{L,i}$ (variable in time) were defined. Initial values for solute concentrations in the biofilm do not significantly influence the model outcome.

Biofilm thickness. The biofilm thickness grows in time, therefore the boundary of the biofilm surface (x=L_F) and boundary layer ($x = L_F + L_{BL}$) move according to equation 6. The biofilm base at x=0 is fixed.

$$\frac{dx}{dt} = u_F|_{x=L_F} \qquad [6]$$

The advective velocity u_F (the velocity at which the biofilm surface grows away from the electrode surface) results from integrating the biomass growth rate over the biofilm thickness [73]:

$$u_F|_{x=L_F} = \int_0^{L_F} \frac{r_X(x)}{c_X} dx \qquad [7]$$

The initial biofilm thickness, $L_{F,0}$, is set to the measured value.

Bulk liquid. The batch-operated aqueous medium was considered ideally mixed, with concentrations $c_{L,i}$ computed from a mole balance in time, including transfer fluxes to/from biofilm, J_{FL}, and gas phase, J_{GL}:

$$\frac{dc_{L,i}}{dt} = J_{FL,i}\frac{A_F}{V_L} + J_{GL,i}\frac{A_{GL}}{V_L} \quad [8]$$

The electrode area covered by biofilm, A_F, the gas/liquid surface, A_{GL}, and the bulk liquid volume, V_L, were all considered constant and known. The diffusion fluxes exchanged with the biofilm are

$$J_{FL,i} = -k_{F,i}\left(c_{L,i} - c_{F,i}\big|_{x=L_F}\right) \quad [9]$$

with mass transfer coefficient $k_F = D_i/L_{BL}$. The fluxes exchanged with the gas phase are similarly expressed as:

$$J_{GL,i} = k_{L,i}\left(c^*_{L,i} - c_{L,i}\right) \quad [10]$$

k_L was given a large value so that the GL transfer is not rate-limiting, while the solubility was computed according to Henry's law as $c^*_{L,i} = H_i c_{G,i}$. Henry coefficients for 25°C were corrected for the actual temperature of 60°C. Concentrations $c_{G,i}$ resulted from mole balances in the gas phase. Initial concentration of dissolved gases were computed from solubility in contact with the gas phase at 2.5 bar, having the given experimental composition.

Gas phase. The mole balances of O_2, H_2 and CO_2 in the gas phase are used to compute the concentrations $c_{G,i}$. The balance equation 11 includes the flux exchanged with the liquid $J_{GL,i}$, periodical flushes with fresh gas with flowrate Q having a given composition $c_{G0,i}$ and gas volume V_G:

$$\frac{dc_{G,i}}{dt} = -J_{GL,i}\frac{A_{GL}}{V_G} + y_i J_{GL,tot}\frac{A_{GL}}{V_G} + \frac{Q(t)}{V_G}\left(c_{G0,i} - c_{G,i}\right) \quad [11]$$

The term containing the mole fraction y_i ensures the condition $y_{O_2} + y_{H_2} + y_{CO_2} = 1$. The flushing gas is modulated by a switch function (1 when flushing for 15 minutes, else 0). The initial and flush gas compositions were computed such that the dissolved O_2 concentration matched the measured values.

Solution method. The system of differential equations 3, 6, 8 and 11 was implemented and solved in COMSOL Multiphysics v6.1 (www.comsol.com). A mesh size of 5 μm was sufficiently accurate.

Parameters. Most of the geometry parameters were measured during the experiments, while the mass transfer boundary layer thickness was taken as a typical value, in the order of 100 μm [73]. Mass transfer parameters for common gases such as O_2, H_2 and CO_2 were in general available from the literature. Microbial kinetics for *Kyrpidia* was in part evaluated during the experiments (maximum growth rate and biomass concentration in the biofilm). Microbial reaction stoichiometry was estimated using the thermodynamic approach from Heijnen and Kleerebezem [49]. The H_2 evolution rate on the electrode was used from the average measured current density for the first 7 days of experimental run, -65 μA cm^{-2}, assuming 100% conversion of electrons to H_2. All parameter values are listed in Table S1 in the supplemental information online.

Thermodynamic derivation of microbial stoichiometry

The derivation of an overall growth stoichiometry is based on the thermodynamic approach presented in Heijnen and Kleerebezem [49].

Catabolic reaction. The microbial growth is based on the energy supplied by a catabolic reaction, in this case involving H_2 as electron donor and O_2 as electron acceptor, with couples H_2/H_2O and O_2/H_2O:

$$-1H_2 - 0.5O_2 + 1H_2O = 0 \quad [12]$$

The Gibbs energy for this reaction in standard biological conditions (01) (i.e., 25 C, pH 7, 1M) is $\Delta G^{01}_{cat} = -237.2$ kJ/reaction. The correction for a temperature of 60 °C can be made with the enthalpy of reaction, $\Delta H^{01}_{cat} = -285.8$ kJ, resulting in $\Delta G^{01}_{cat,60} = \Delta G^{01}_{cat,25} \cdot \frac{60+273}{25+273} + \Delta H^{01}_{cat,25} \cdot \frac{25-60}{25+273} = -231.5$ kJ. Finally, corrections for the partial pressure of gases lead to $\Delta G^{1}_{cat,60} = -221$ kJ / reaction.

Anabolic reaction. This includes the C-source, in this case HCO_3^- and a nitrogen source as ammonium:

$$-2.1H_2 - 1HCO_3^- - 0.2NH_4^+ - 0.8H^+ + 2.5H_2O + 1CH_{1.8}O_{0.5}N_{0.2} = 0 \quad [13]$$

The Gibbs energy in standard biological conditions is $\Delta G^{01}_{an} = -25.3$ kJ / reaction, while with temperature correction it is $\Delta G^{01}_{an,T} = -18$ kJ, as concentration corrections resulting in $\Delta G_{an,T}$ very close to zero.

The Gibbs energy dissipation when using a carbon source with C=1 (as CO_2 is here) and degree of reduction of zero ($\gamma_{CO2} = 1 \cdot 4 + 2 \cdot (-2) = 0$) is estimated as $Y_G^{max} = -980$ kJ/C mol X. See eq. [20] in [49] for autotrophic growth without reversed electron transfer RET, as H_2 can deliver enough energy. The results depend heavily on this dissipation energy.

This allows to compute a catabolism multiplication factor *f*, meaning how many catabolic reactions must be executed so that enough energy is produced to run one anabolic reaction.

$$f = \frac{-986-0}{-221} \simeq 4.45 \quad [14]$$

The overall growth stoichiometry results by summation of 4.45 x (catabolism) + anabolism:

$$-(2.1 + f)H_2 - 0.5fO_2 - 1HCO_3^- - 0.2NH_4^+ - 0.8H^+ + (2.5 + f)H_2O + 1CH_{1.8}O_{0.5}N_{0.2} = 0 \quad [15]$$

giving finally:

$$-6.5H_2 - 2.22O_2 - 1HCO_3^- - 0.2NH_4^+ - 0.8H^+ + 6.9H_2O + 1CH_{1.8}O_{0.5}N_{0.2} = 0 \quad [16]$$

Therefore, the biomass growth yields on the three substrates were taken as

$$Y_{HX} = 6.5 \text{ mol } H_2/\text{C–mol X}, \quad Y_{OX} = 2.22 \text{ mol } O_2/\text{C–mol X}, Y_{CX} = 1 \text{ mol } CO_2/\text{C–mol X} \quad [17]$$